Palacký University Olomouc
Faculty of Science

Department of Optics

Construction and experimental demonstration of a four-photon source

Master's Thesis

Daniela Slouková

Study programme:	N1701 Physics
Field of study:	Optics and Optoelectronics
Form of study:	Full-time
Supervisor:	Vojtěch Trávníček, PhD
Workplace:	Joint Laboratory of Optics
Thesis submitted on:	

Univerzita palackého
Přírodovědecká fakulta

Katedra optiky

Konstrukce a experimentální demonstrace čtyřfotonového zdroje

Diplomová práce

Daniela Slouková

Studijní program:	N1701 Fyzika
Obor:	Optika a optoelektronika
Forma studia:	Prezenční
Vedoucí:	Mgr. Vojtěch Trávníček, Ph.D.
Školící pracoviště:	Společná laboratoř optiky
Práce odevzdána dne:	

Abstract

The aim of the thesis is to build a four-photon source and demonstrate its properties. The source we present is based on nonlinear optical process of spontaneous parametric down-conversion. The multiple-photon source is essential and conditional for implementation of numerous quantum gates and quantum communication protocols such as programmable controlled-phase gate and entanglement swapping. We not only focus on the description of the optical components used but also on the alignment process of the experiment. We demonstrate experimentally the Hong-Ou-Mandel interference to display the functionality of the source.

Keywords

`Quantum Information Processing, Nonlinear Optics, Parametric Down-conversion, Second Harmonic Generation`

Acknowledgments

I would like to sincerely express my deepest gratitude to my supervisor Vojtěch Trávníček, PhD, for all the advice he gave me, for his patience and the time he devoted to our consultations, construction of experiment and measurements in the lab. I would also like to thank the Assoc. Prof. Karel Lemr, PhD, for his efforts and ideas while construction of our experiment. I also thank all the colleagues from Joint Laboratory of Optics and Department of Optics, who were helpful and supportive throughout realization of experiment. To my dear friends, especially Anežka and my sister, I want to express my sincerest appreciation for their unwavering support that made all challenges more manageable. A really special thanks belong to my family and my husband for all the support throughout my studies.

I gratefully acknowledge the support from the project IGA_PrF_2022_004 and IGA_PrF_2023_005 of Palacky University.

Declaration

I hereby declare that I have written this Master's Thesis by myself, while being supervised by Vojtěch Trávníček, PhD.

Contents

Chapter 1

Introduction

In the beginning of 20th century, Max Planck proposed that energy is not emitted or absorbed continuously, but rather in discrete quanta. This idea emerged from his efforts to explain the spectrum of blackbody radiation, a problem that classical physics had struggled to solve [1]. It was further developed and expanded upon by physicists such as Albert Einstein, Niels Bohr, Werner Heisenberg, and Erwin Schrödinger, among others [2].

Photons (as quanta of light) possess inherent properties such as polarization, phase, and momentum, which can be used to represent quantum information. The states of light are important platforms in quantum information processing (QIP) and quantum communications [3]. In quantum information processing, quantum states are fundamental for encoding and processing information. Qubits (known as quantum bits) are the basic units of quantum information. Unlike classical bits, which can theoretically exist only in one of two states (0 or 1), assumption of superposition principle allows qubit to exist in a superposition of both states simultaneously. This property enables quantum computers to explore multiple possibilities in parallel, potentially leading to exponential speedup for specific algorithms in comparison to their classical counterparts [4]. Through polarization manipulation, qubits can be precisely

encoded into photons. In polarization encoding, the two logical basis states $|0\rangle$ and $|1\rangle$ represent horizontal and vertical polarization, respectively [5].

Using photons as quantum information carriers offers significant advantages owing to their easy manipulation by linear optics platform (by optical components such as mirrors, beam splitters, and phase shifters) and their speed of propagation with minimal tendency of interaction with environment, e.g. qubits have long decoherence time [6]. The ability to travel through space with minimal decoherence ensures efficient transmission of quantum information over long distances, essential for applications such as quantum key distribution or repeater [7, 8]. For numerous quantum communication experiments and protocols, besides superposition principle, an entanglement phenomenon plays a key role as well, e.g. in dense coding or quantum teleportation [9, 5]. Quantum entanglement contributed significantly to the advancement of quantum communication research [10]. It is a property occurring between two or more particles so that the state of one particle is dependent on the state of another. As a result, the quantum state of the particle cannot be described independently on another, regardless of the distance separating them. In 1987, the Hong-Ou-Mandel (HOM) experiment demonstrated the two-photon interference phenomenon at the University of Rochester. The experiment is now widely used in many quantum optical experiments [11].

With the invention and initial demonstration of the laser in the 1960s, the potential for conducting quantum nonlinear experiments expanded significantly [12]. This was primarily due to the high intensities, or strong fields, generated by lasers, which enabled the observation of nonlinear processes occurring in materials that exhibit strong nonlinear optical properties. Nowadays, lasers have indispensable role in various fields, they find application e.g. in scientific research, including applications like spectroscopy, holography, and, notably, in quantum optical experiments.

The main purpose of this thesis is to construct a four-photon source based on spontaneous parametric down-conversion (SPDC) in β-baryum borate (BBO) crystal and to discuss its properties. Multiphoton source is significant in quantum optics, quantum information processing and quantum communications, as it enables the investigation of complex quantum phenomena and the implementation of various quantum protocols [13, 14]. For this reason, precision in preparation, manipulation and detection of the state of light is required. Our goal is to construct a source that generates four photons. A suitable solution is to generate two correlated photon pairs by the process of SPDC, which enables the generation of photon pairs exhibiting quantum correlations, and in the right configuration gives us the possibility to generate entangled photons. In the outset of this thesis in Chapter 2, methods and tools that are needed for construction of the source are briefly introduced. Chapter 3 describes the setup and optical components used for construction of the source, as well as the adjustment processes. The diagnostic methods based on the HOM interference are defined as well. The results of HOM interference measurements are presented and discussed in Chapter 4. The final chapter concludes the work and provides a summary of the main points discussed.

Chapter 2

Methods and Tools

Four-photon source is a versatile tool for multiple quantum optical protocols and experiments such as router, repeater or quantum key distribution. For the realization of such a source, it is practical to use some of the nonlinear optical processes. In practice, the processes of spontaneous parametric down-conversion and second-harmonic generation (SHG) are used. This chapter is devoted to description of these processes, principles and simple optical tools we use in our setup.

2.1 Qubits

In general, a qubit is a two-level quantum system. Unlike classical bits, which can exist in one of two states (0 or 1), qubits can exist in a superposition of both states simultaneously. As the fundamental units of quantum information, qubits can be used to represent quantum states. There are several methods available for encoding quantum information e.g. one can encode into frequency, orbital angular momentum, time or space. Another method for encoding quantum information is through the use of photons and their polarization states. In polarization encoding, the two basis states $|0\rangle$ and $|1\rangle$ represent horizontal and vertical polarization, respectively. To visualise qubits, it is convenient to use the Bloch sphere, where, as depicted in Figure 2.1, the $|0\rangle$ and $|1\rangle$ polarization

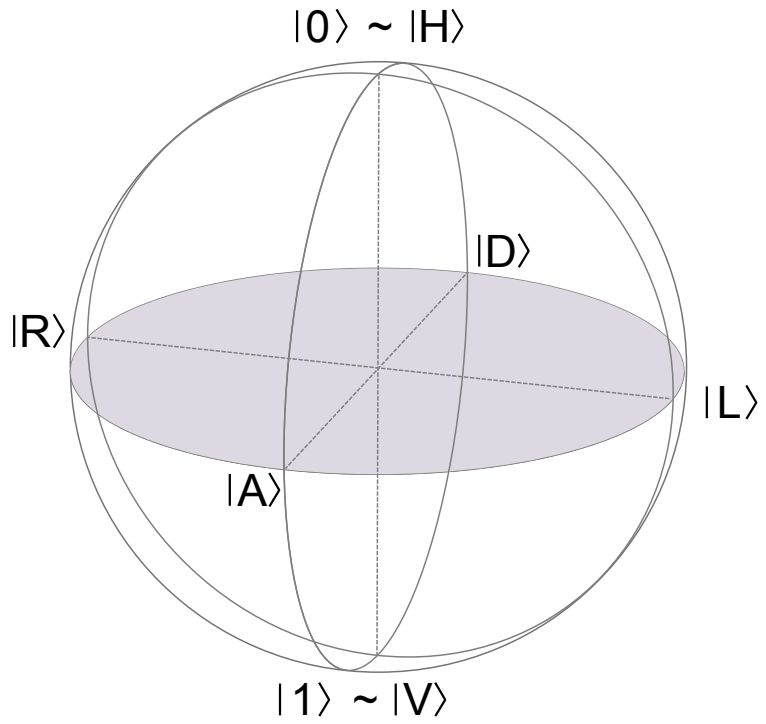

Figure 2.1: Bloch sphere as the geometrical representation of polarization of one qubit. The polarizations are marked as follows: $|0\rangle$ – horizontal, $|\ 1\ \rangle$ – vertical, $|R\rangle$ – right-hand circular, $|L\rangle$ – left-hand circular, $|D\rangle$ – diagonal and $|A\rangle$ – anti-diagonal polarization.

states reside at the north and the south pole and their superpositions (i.e. pure states) lie on the surface of the sphere, therefore mixed states reside in the interior of the Bloch sphere. Formally, qubit can be defined as a normalized vector $|\psi\rangle$ in the two-dimensional Hilbert space

$$|\psi\rangle = \alpha|0\rangle + \beta|1\rangle, \tag{2.1}$$

where α and β are complex numbers and are called probability amplitudes, which are normalized so that the condition

$$|\alpha|^2 + |\beta|^2 = 1 \tag{2.2}$$

is satisfied.

2.2 Laser

Laser (i.e. Light Amplification by Stimulated Emission of Radiation) is a coherent source of light with narrow frequency band. We employed the type of Ti:Sapphire femtosecond laser as the strong pump source, operating at the central wavelength of 826 nm in our experiment. A Ti:Sapphire laser is a type of solid-state laser that uses a crystal of Sapphire (Al_2O_3) doped with Titanium ions (Ti^{3+}) as the gain medium. Ti:sapphire lasers are known for their tunability over a broad range of wavelengths in the near-IR region, high power output, and ultrashort pulse duration. The tuning range is typically from about 650 nm to 1100 nm. The main reasons for choosing the Ti:Sapphire laser are the large laser mode volumes and the mode-locking capability, enabling the generation of pulses with ultrashort duration and high power output [15]. Therefore, we prefer to use a source that generates photons in the near-IR region, although a conversion down to lower wavelengths is necessary due to the use of silicon based single-photon detectors.

2.3 Description of Nonlinear Optical Interactions

With the invention of laser, the intensity of the optical field interacting with matter rapidly increased up to $10^{12}\ \mathrm{V \cdot m^{-1}}$. Since the nonlinear optical properties of a given optical medium manifested when interacting with such strong field, it was observed and confirmed that the material constants of given optical medium vary depending on the intensity of the incident field. The description of interactions with nonlinear material is based on the Maxwell's equations for the nonlinear medium. Let us simplify the Maxwell's equations for the case when no free charges and

currents are present so the equations are in the form:

$$\begin{aligned} \nabla \cdot \overrightarrow{D} &= 0 & \nabla \cdot \overrightarrow{B} &= 0 \\ \nabla \times \overrightarrow{E} &= -\frac{\partial \overrightarrow{B}}{\partial t} & \nabla \times \overrightarrow{H} &= \frac{\partial \overrightarrow{D}}{\partial t}. \end{aligned} \tag{2.3}$$

We cannot forget to mention the material relations, which can be for non-magnetic material written as

$$\overrightarrow{B} = \mu_0 \overrightarrow{H} \qquad \overrightarrow{D} = \epsilon_0 \overrightarrow{E} + \overrightarrow{P}, \tag{2.4}$$

where the material polarization $\overrightarrow{P} = \epsilon_0 \chi(E) \overrightarrow{E} = \overrightarrow{P}_{lin} + \overrightarrow{P}_{NL}$ (or expressed by its elements $P_i = \epsilon_0 \chi_{ij} E_j$) in general includes also nonlinear contribution. The dependence of susceptibility χ on E is further important for the transition to nonlinear optics. We can develop $\overrightarrow{P}$ into a Taylor series

$$P_i = \epsilon_0 [\chi^{(1)}_{ij} E_j + \chi^{(2)}_{ijk} E_j E_k + \chi^{(3)}_{ijkl} E_j E_k E_l],$$

where $\chi^{(1)}$ is a 2nd order tensor corresponding to a linear contribution and $\chi^{(2)}$ and $\chi^{(3)}$ are higher order tensors corresponding to the nonlinear contributions. The expressions $\epsilon_0 \chi^{(2)}_{ijk} E_j E_k$ and $\epsilon_0 \chi^{(3)}_{ijkl} E_j E_k E_l$ represents the nonlinear polarization corresponding to the optical processes of the second and third order, respectively. Note that generally χ includes complex numbers. Nonlinear optical processes can be divided into two sections as parametric and non-parametric processes. In parametric processes, the interacting field does not affect the quantum state of the material. This means that the photon energy meets the condition of energy conservation and can be described using the real part of susceptibility. On the other hand, non-parametric processes are described by the complex part of susceptibility. In this case, the condition of energy conservation is not met, which means that energy can be transmitted into and out of the material. [16]

Using equations (2.3) and (2.4) and interchanging the order of space and time derivatives, it is easy to derive wave equation describing the

propagation of light through a nonlinear optical medium

$$\nabla^2 \overrightarrow{E} - \frac{1}{c^2}\frac{\partial^2}{\partial t^2}\overrightarrow{E} = \frac{1}{\epsilon_0 c^2}\frac{\partial^2 \overrightarrow{P}}{\partial t^2}, \tag{2.5}$$

where $\frac{1}{c^2} = \mu_0 \epsilon_0$.

2.3.1 SHG

As we mentioned earlier in this chapter (see Sec. 2.2), due to the use of silicon single-photon detectors, it is useful and also more energetically efficient to generate higher wavelength output and then transform it down to the desired wavelength. To achieve the transformation, it is convenient to use the process of second-harmonic generation. SHG is a parametric nonlinear optical process for which the second-order susceptibility $\chi^{(2)}$ is nonzero, so that the nonlinear susceptibility obeys the condition of full permutation symmetry. According to a simple scheme in part (a) of Figure 2.2, input beam (e.g. laser beam) at frequency ω is incident upon a crystal, where the second-harmonic frequency 2ω is generated. Typically, a residual of the fundamental frequency remains present at the crystal output, which may require filtering out. In part (b) of Figure 2.2 one can see the principle of SHG, where the two photons at the same frequency ω interact and decay, creating a photon of frequency 2ω simultaneously. The dashed lines represent virtual energy levels. SHG, often called as frequency doubling, can also be understood in a very similar way to another nonlinear process known as sum-frequency generation. Here, the two beams at different frequencies interact resulting in the beam at frequency corresponding to the sum of the input frequencies.

The process of SHG can be mathematically described by coupled-amplitude equations. These equations are derived by substituting corresponding expressions of $\overrightarrow{E}$ and $\overrightarrow{P}$ into the wave equation describing the interactions with nonlinear medium (see Eq. (2.5)) with the slowly varying envelope approximation (so that the second derivatives can be

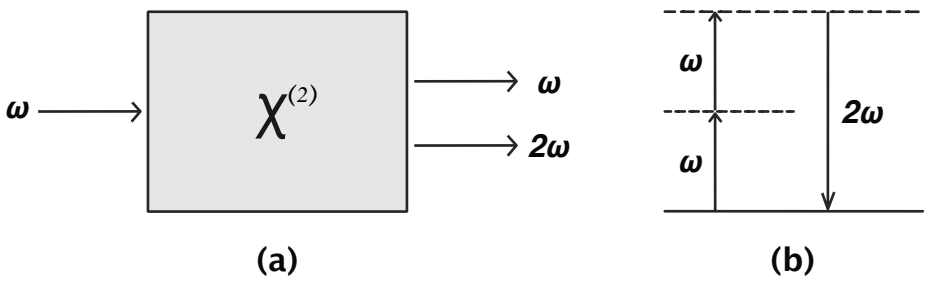

Figure 2.2: (a) Geometry of second-harmonic generation. (b) Energy-level diagram that describes second-harmonic generation.

neglected). Generally $\overrightarrow{E}$ can be written as $E_i(z,t) = E_i(z) \cdot e^{-i\omega t}$, where $E_i(z) = A_i \cdot e^{ikz}$. So if we substitute into the wave equation, one can obtain the coupled-amplitude equations

$$\begin{aligned} \frac{dA_1}{dz} &= \frac{2i\omega_1^2 d_{eff}}{k_1 c^2} A_2 A_1^* e^{-i(2k_1 - k_2)z} \\ \frac{dA_2}{dz} &= \frac{2i\omega_2^2 d_{eff}}{k_2 c^2} A_1^2 e^{i(2k_1 - k_2)z}, \end{aligned} \tag{2.6}$$

where $A_{1,2}$ are the electric field amplitudes, $\omega_{1,2}$ stands for frequencies, c corresponds to the velocity of light, $k_{1,2}$ are wave vectors, i imaginary unit and parameter d_{eff} is a nonlinear coefficient of material related to the nonlinear optical susceptibility $d_{eff} = \frac{1}{2}\chi^{(2)}$. In the exponential of the coupled-amplitude equations arises so-called phase matching condition, often expressed in terms of the wave vector mismatch

$$\Delta k = 2k_1 - k_2 = 0. \tag{2.7}$$

Under the assumption of complete phase-matching, the process of SHG can be so efficient so that almost all of the incident power at frequency ω is transformed up to the 2ω when passing through the nonlinear medium. In an isotropic media in the regime of normal dispersion, where the refractive index of material increases with frequency, the process of SHG is clearly not possible because $n(\omega)$ increases with ω (for the case of SHG

should be $n(\omega_1) = n(2\omega_1) = n(\omega_2)$). To overcome this problem, one might use anomalous dispersion, i.e. decreasing of refractive index with increasing frequency. However, anomalous dispersion often occurs in materials that exhibit significant absorption, which can lead to significant losses in the generated second harmonic signal, reducing the efficiency of the SHG process. If one wants to stay off the anomalous dispersion, one can make use of the properties of an anisotropic media, where the refractive index varies with factors such as polarization, propagation direction, and frequency for specific angles and wavelengths. For this case, it is common to use the birefringent material. Birefringence is an optical property of certain materials in which light waves traveling through the material experience two different refractive indices often denoted as ordinary n_o and extraordinary n_e index. Hence, when a beam enters a birefringent material, it splits into two polarized beams with generally different velocities and directions [16]. Its controlling is essential in many optical applications e.g. in communications, the usage of stress induced birefringence is common in production of polarization maintaining fibers [17]. One has to take into account that the property of birefringence is temperature-dependent and thus the temperature must be controlled. Phase matching condition is therefore a crucial condition for efficient generation, therefore a lot of resources and effort are devoted to production of this finely tuned crystals. Nevertheless, for the materials which do not experience birefringence (or not enough), one can use the technique of quasi-phase-matching to enhance the nonlinear processes efficiency. This method relies on periodically inverting the orientation of the crystal axis. Such crystal structure is then called as periodically-poled.

2.3.2 SPDC

A common way to generate photon pairs is the process known as spontaneous parametric down-conversion. SPDC is a nonlinear optical process that occurs in materials with second order optical nonlinearity, in which

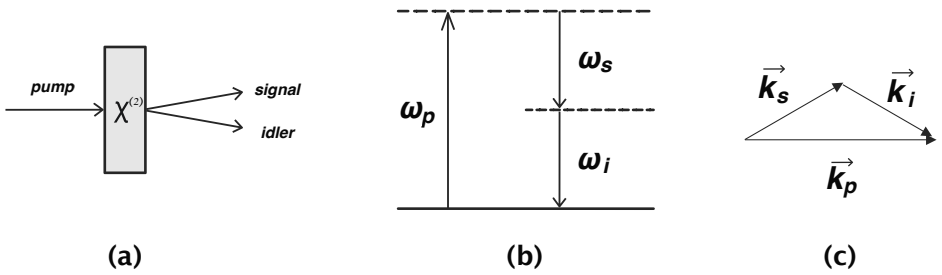

Figure 2.3: (a) Geometrical interpretation of SPDC, (b) energy and (c) momentum conservation.

a strong pump photon (p) (on higher frequency) is spontaneously transformed into a pair of lower-frequency photons. These photons, referred as signal and idler (s and i) are time correlated (created at the same time) and, in fact, can be entangled.

The process of SPDC requires similar conditions to be satisfied for efficient generation as SHG. The phase matching condition for SPDC involves the conservation of energy and momentum as depicted in Figure 2.3. The frequency of the pumping photon must be the same as the sum of the signal and idler photon frequencies $\omega_p = \omega_s + \omega_i$. The momentum conservation condition in a general form can be expressed as a vector equation $\overrightarrow{k_p} = \overrightarrow{k_s} + \overrightarrow{k_i}$, where $\overrightarrow{k}$ stands for the wave vectors. In case of $\omega_s = \omega_i$ the process is completely degenerated.

There are several types of SPDC that differ in polarization with respect to the pumping beam. These types are described below and depicted in Figures 2.4, 2.5 and 2.6. Presented schemes show only non-collinear cases of SPDC, but generally, SPDC can be collinear.

Type I

The two generated photons have parallel polarization, perpendicular to the polarization of the pumping photon and can be found on a cone with

the axis that is equal to the propagation direction of the pumping beam. Photons from the same photon pair can be found on the opposite sides of the cone surface (see Figure 2.4). Photons generated using only one crystal for Type I SPDC process in fact cannot be directly polarization entangled. Polarization entanglement could be achieved afterwards by post-selection [18].

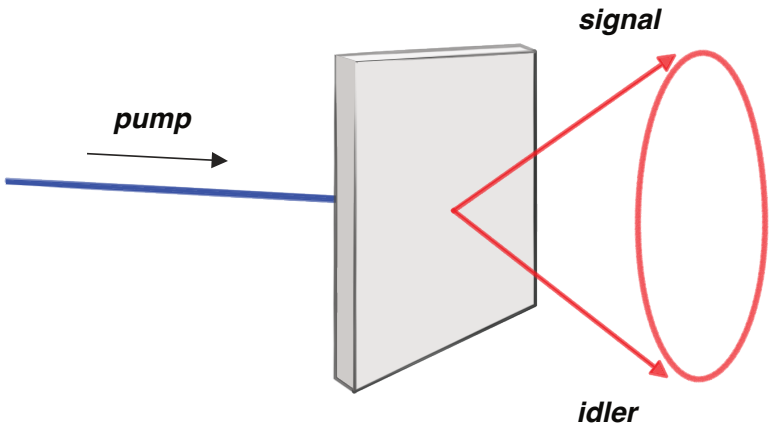

Figure 2.4: The Type I SPDC, where the generated photons have polarization perpendicular to the polarization of the pumping beam.

Type II

The two generated photon pairs have mutually perpendicular polarization. The photons are generated from the crystal into the two cones with axis different to propagation direction of the pumping beam. Photons that lie in the intersections of the two cones surfaces are entangled in polarization, because of the non-distinguishability of the signal and idler photons in these intersections. The alignment of the cones axes can vary based on the orientation of the main axis of the non-linear crystal with respect to the interface and the direction of the pump beam. As a result, these cones may intersect at zero, one, or two points (see Figure 2.5).

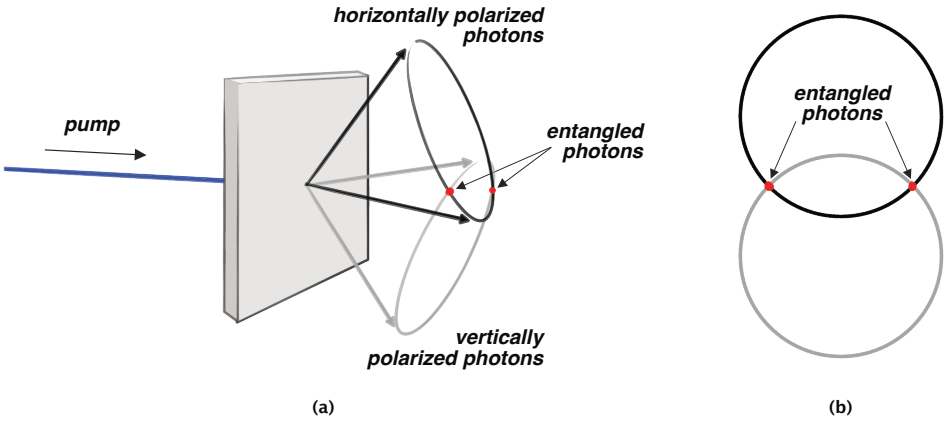

Figure 2.5: (a) The Type II SPDC, where the entangled photons lie on the intersection of the two cones and (b) the projection of the intersecting beams emerging from the SPDC.

Kwiat source

The Kwiat source (as depicted in Figure 2.6) represents another way in order to generate photons that are entangled in polarization. In this configuration, a cascade of two crystals cut for Type I SPDC process are arranged with their optical axes oriented so that their planes are mutually rotated by 90°. Thus the crystals generate a photon pair with mutually orthogonal polarization. One of the crystals converts horizontally polarized pump beam into vertically polarized photon pairs and the second crystal transforms the vertically polarized pump beam into horizontally polarized photon pairs. Then, when pumping by a generally polarized light beam, polarization entangled state

$$|\psi\rangle = \cos\alpha|HH\rangle + e^{i\phi}\sin\alpha|VV\rangle \tag{2.8}$$

is generated. Here the $\tan\alpha$ is the ratio of amplitudes in the horizontal and vertical polarization modes of the pumping beam and ϕ corresponds to their mutual phase-shift. [19]

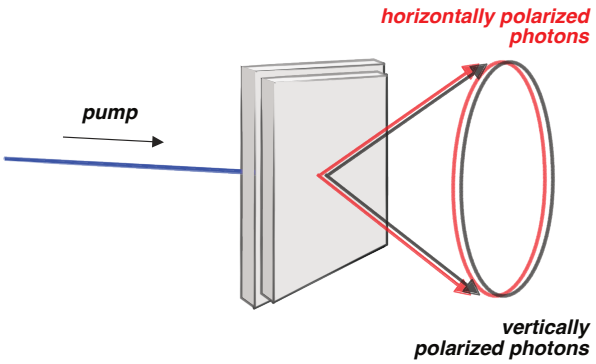

Figure 2.6: The scheme for the Kwiat source generating entangled photons.

2.4 Beam splitter (BS)

Beam splitters play an important role in quantum-optical experiments, allowing for interaction of two modes of light. They are perfect tools for demonstration of the quantum nature of light and are used in various quantum-optical experiments. BS can be simply understood as a device where two incident light modes interfere to produce two output beams. In quantum theory, the principle can be explained in terms of Fock states, which are the quantum states representing a fixed number of identical particles. Electric field can be represented by creation and anihilation operators $\hat{a}$ and $\hat{a}^\dagger$. Their commutation relations are

$$[\hat{a}_m, \hat{a}_n^\dagger] = \delta_{m,n} \tag{2.9}$$

$$[\hat{a}_m, \hat{a}_n] = 0 \tag{2.10}$$

$$[\hat{a}_m^\dagger, \hat{a}_n^\dagger] = 0. \tag{2.11}$$

Using these operators, one can define the number operator

$$\hat{n}_k = \hat{a}_k^\dagger \hat{a}_k \tag{2.12}$$

that occurs in the Hamiltonian for the electromagnetic field

$$H = \sum_{k=1}^{\infty} \hbar\omega_k(\hat{n}_k + \frac{1}{2}), \tag{2.13}$$

where $\hbar$ is the reduced Planck constant.

Fock states are then eigenstates of the number operator

$$\hat{n}_k|n_k\rangle = n_k|n_k\rangle. \tag{2.14}$$

The creation and anihilation operators act on the Fock states as follows:

$$\hat{a}_k|n_k\rangle = \sqrt{n_k}|n_k - 1\rangle \tag{2.15}$$

$$\hat{a}_k^\dagger|n_k\rangle = \sqrt{n_k + 1}|n_k + 1\rangle, \tag{2.16}$$

hence

$$|n_k\rangle = \frac{(\hat{a}_k^\dagger)^{n_k}}{\sqrt{n_k!}}|0\rangle, \tag{2.17}$$

where $|0\rangle$ is a vacuum state. As depicted in Figure 2.7, the ports of the

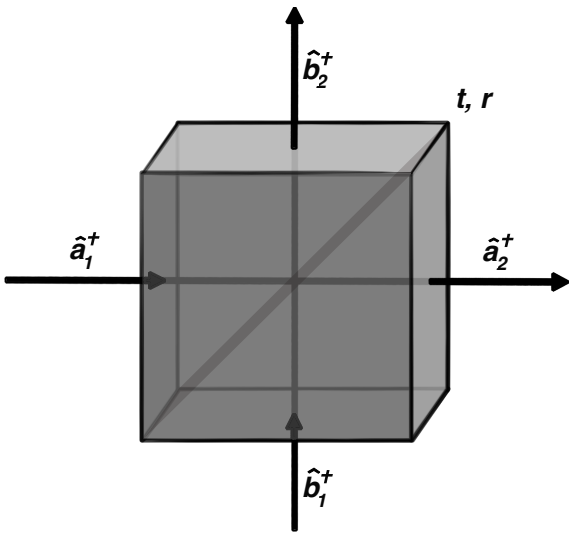

Figure 2.7: The scheme of the beam splitter.

beam splitter are represented by a photon number state with action of

a creation operator (see Eq. (2.16)). Therefore the two input modes are denoted as $\hat{a}_1, \hat{b}_1$ and the output modes $\hat{a}_2, \hat{b}_2$. Under the assumption of the lossless beam splitter, unitary transformation is realized

$$\begin{pmatrix} \hat{a}_2^\dagger \\ \hat{b}_2^\dagger \end{pmatrix} = \begin{pmatrix} t & r \\ -r & t \end{pmatrix} \cdot \begin{pmatrix} \hat{a}_1^\dagger \\ \hat{b}_2^\dagger \end{pmatrix}, \tag{2.18}$$

where t and r the are complex numbers known as the transmission and reflection coefficients that must satisfy

$$|t|^2 + |r|^2 = 1 \qquad \text{and} \qquad r^* t + r t^* = 0. \tag{2.19}$$

If we start from the Fock state $|0,0\rangle$ and add the photon in the input ports of the beam splitter, we get

$$|1,1\rangle = \hat{a}_2^\dagger \hat{b}_2^\dagger |0,0\rangle \tag{2.20}$$

that can be further, with making use of the equation (2.18), rewritten as

$$(t\hat{a}_1^\dagger + r\hat{b}_1^\dagger)(t\hat{b}_1^\dagger - r\hat{a}_1^\dagger)|0,0\rangle = \sqrt{2}tr(|0,2\rangle - |2,0\rangle) + (t^2 - r^2)|1,1\rangle. \tag{2.21}$$

When we assume of $t^2 = r^2 = \frac{1}{2}$ (i.e. 50:50 beam splitter), the expression (2.21) reduces to

$$\frac{1}{\sqrt{2}}(|0,2\rangle - |2,0\rangle). \tag{2.22}$$

This situation corresponds to a well-known phenomenon called two-photon bunching, or Hong-Ou-Mandel interference (for measurement description of HOM interference see Sec. 2.7). In our experiment, we use a fiber beam splitter (FBS), which is a 2×2 single-mode fiber optic coupler with a 50:50 splitting ratio. The simplified scheme of the coupler is depicted in Figure 2.8.

2.5 Beam displacer (BD)

Beam displacer separates incident light into two beams. BDs are manufactured from e.g. calcite, which is a birefringent material that causes the

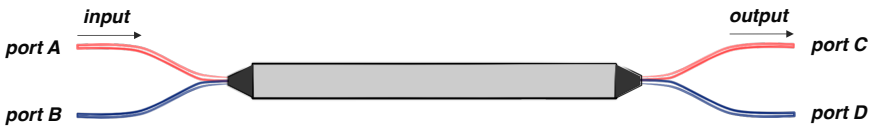

Figure 2.8: The scheme of a fiber beam splitter.

light with perpendicular polarization to a plane defined by the optical axis and direction of propagation to experience different refraction index than light that has parallel polarization to the plane. Thus, the incident unpolarized light beam is laterally separated into two mutually displaced beams (typically in a range of millimeters) that have orthogonal polarization and are parallel to each other. The scheme of the beam displacer is depicted in Figure 2.9. According to the scheme, displacement d can be thus calculated as

$$d = L \cdot \tan \alpha \tag{2.23}$$

and $\tan \alpha$ expressed as

$$\tan \alpha = \left(1 - \frac{n_0^2}{n_e^2}\right) \cdot \frac{\tan \theta}{1 + \frac{n_0^2}{n_e^2} \cdot \tan^2 \theta}, \tag{2.24}$$

where n_0 and n_e are the ordinary and extraordinary indices of refraction, respectively, and θ stands for the optical axis of the beam displacer.

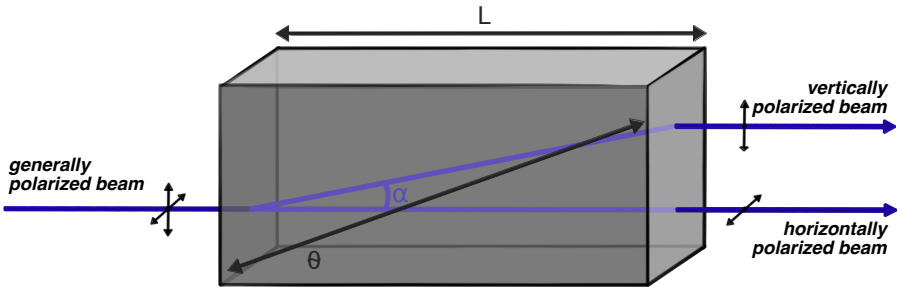

Figure 2.9: The scheme of the beam displacer, separating the vertical and horizontal polarization component of the light.

2.6 Detectors

All detectors used in our setup are single-photon avalanche photodiodes (APD) working in Geiger mode. APD, in fact, is a modified p-i-n diode (for the scheme of such p-i-n diode see Fig. 2.10), operated under reverse bias voltage higher than destructive, converting an incident signal into electric signal. Since the operating reverse bias is higher than destructive, one needs to quench the circuit to prevent its destruction. There are two types of quenching, active and passive. In case of active quenching circuit, there is an electrical circuit measuring the current and circuit then quickly reduces the bias voltage to below breakdown and returns the bias voltage to its original value, higher than destructive. Passive quenching includes a single resistor in the series and the voltage is developed across the resistor and the detector. After the detection, the resistance of the detector decreases. Then the bias slowly returns back to the initial voltage to be ready to detect again. Detectors using the passive quenching have lower repetition frequency, but they are more resistant to an illumination of higher number of photons. We are using detectors with active quench circuit and detection efficiency about 65% [20].

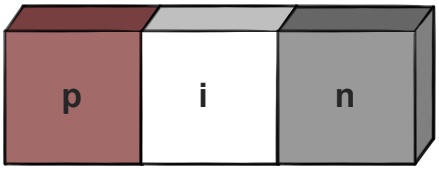

Figure 2.10: Conceptual scheme of p-i-n diode, consisting of extrinsic and intrinsic semiconductors. Extrinsic semiconductors are those that have to be doped. Dopants are classified as electron donors or acceptors. Semiconductors doped with acceptors are known as p-type and those doped with donors are called n-type semiconductors. Therefore labels p, n and i stand for the p-type, n-type and intrinsic semiconductors, respectively. The p-i-n diodes only detect incoming photons in the depleted region, which is unlike the elementary p-n junction expanded by placing the intrinsic semiconductor between the p-type and n-type.

2.7 HOM interference

To observe HOM interference, the two photons are directed onto a 50:50 beam splitter, each at one input port of the BS. If they are indistinguishable in all degrees of freedom, the overlap of the photons on the BS is perfect and the effect known as two-photon bunching occurs so the two interacting photons will always exit the BS together in the same output mode (no matter which mode it would be). That means there is no chance to detect a coincidence (i.e. simultaneous detection event) at both output ports, because at one of them, there will always be a vacuum state, so the detector will not register detection event. This phenomenon is mathematically described above in the section 2.4. Note that in the case of polarization entangled photons in a singlet Bell state [21]

$$|\psi\rangle = \frac{1}{\sqrt{2}} \left(|01\rangle - |10\rangle \right), \tag{2.25}$$

one needs to use a polarization beam splitter and anti-bunching occurs [22].

As written in the outset of the section 2.3, for parametric processes the energy of photons is preserved so that the state of the crystal remains unchanged. Thus there are only the optical fields interacting. The time correlation of signal and idler photons generated through SPDC is essential for observing HOM effect. In our setup, we couple the generated photons into the single-mode optical fibers and let them interfere on a fiber beam splitter. By laterally moving one of the fiber couplers and monitoring coincidence counts, we are able to find time overlap and, thus, can observe HOM interference. Coincidence measurements are performed at the output ports of the beam splitter (i.e. both detectors register a photon simultaneously). The perfect overlap means the coincidence counts should theoretically drop down to zero.

Visibility of the HOM interference denoted as V indicates the indistinguishability of generated photon pairs. Visibility is defined as

$$V = \frac{C_{max} - C_{min}}{C_{max} + C_{min}}, \tag{2.26}$$

where C_{max} and C_{min} are the rates of maximal and minimal coincidence counts, respectively.

Chapter 3

Experiment

In this chapter, the experimental arrangement for construction of a four-photon source (4PS) with all components used is introduced and described in detail. Moreover, the whole adjusting process is mentioned.

Strong pump source In our setup, MaiTai laser system is used as the pumping beam, that is Ti:Sapphire femtosecond laser with repetition rate of (80 ± 1) MHz and tunable wavelength range from 690 nm up to 1040 nm. The laser is operated using MaiTai control software provided by Spectra-Physics (or can be controlled remotely via e.g. terminal), where one can select desired wavelength to be emitted and tune the strength of laser pumping [23]. The main advantage of laser control through the computer app is the simplicity of operating the system, i.e. tuning the laser wavelength and the strength of pumping. Controlling the laser through the computer is both the advantage and disadvantage, because if the program does not respond for about 3 seconds, the laser turns off and thus, it ruins the whole measurement. Decreasing the strength of pumping has also its limits, typically the laser becomes unstable and one has to check up the laser stability and that it has not dropped out of the pulsing regime.

SHG unit To perform second-harmonic generation process, we use the GWU-SHG series for SpectraPhysics by GWU-Lasertechnik. The core of the SHG unit consist of nonlinear optical crystal. When all the necessary conditions are satisfied, the frequency of the input beam is doubled. The condition of phase matching was set manually by rotating the crystal (i.e. setting the correct angle of the crystal with respect to the input beam) and looking for the maximum value of output power at desired wavelength. We measured the power of the doubled frequency beam by the use of the power meter PM100D by Thorlabs [24] with Thermal power sensor S302C [25]. Typical photo-diodes have limit of 50 mW of incident optical power, whereas thermal power sensor enables power measurements up to 5 W in free space. As well as the laser (see paragraph 3), SHG unit (angle tuning) can be operated using GWU software.

Kwiat source As written in subsection 2.3.2, Kwiat source is a cascade of two BBO (beta-barium borate) crystals. In the presented experiment crystals with dimensions of $8 \times 8 \times 0.61$mm were used. The cut angle of both crystals is $29.1°$, so that the resulting angle between propagation directions of the pump and generated photons is about 4 degrees.

Interference filters Limiting the spread of the spectrum is often realized by interference filters (IF). Their principle is in general based on a Fabry-Perot resonator consisting of two partially transparent mirrors separated by an air gap. The interference of reflected beams inside the resonator provides the wavelength selection. When the interference is constructive, the transmission is maximal. Various spectral widths of IF ($1.5, 3, 5$ and 10 nm) were used in our experiment.

Coincidence counter To verify that the generated photons are detected at the same time, one needs any coincidence (i.e. simultane-

ous detection events by two or more detectors) logic to be connected to the detectors. Our choice was to use the coincidence counter by Tausand electronics, which allows to adjust settings. One is able to control settings such as sampling time (from 1 ms up to 1000 s) or coincidence window (from 2 ns to 10 μs). To allow time compensating, we can set delay per channel up to 100 ns and to avoid after-pulsing, sleep time per channel up to 100 ns. The mini-USB port on the rear panel can be used for configuration and data collection. There are Python, Matlab and LabView libraries available. We made the decision to utilize a `PyAbacus - Tausand AB1000` library for Python. [26]

Polarization controller A polarization controller is a device used in optics and telecommunications enabling control of the polarization state of light propagating through an optical system. In our setup, we use polarization controller with 3 paddles. Its operational principle is based on a birefringence that is stress-induced, achieved by wrapping the fiber around the three spools (one or two-times). By this winding process we effectivelly created wave plates of $\lambda/4$, $\lambda/2$ and $\lambda/4$ respectively. Consequently, an arbitrary input polarization state can be adjusted by rotating the paddles.

3.1 Setup description

As one can see in the model of our setup, which is depicted in Figure 3.1, the pumping laser beam enters the SHG unit, converting its wavelength from 826 nm down to 413 nm. Then, the laser beam at 413 nm passes through a half-wave plate ($\mathbf{HWP}_1$) that allows manipulation with the polarization state of the light. The beam continues through the set of beam displacers with a half-wave plate placed between them ($\mathbf{HWP}_2$). This construction of the two beam displacers with $\lambda/2$ wave plate inserted represents a form of a Mach-Zehnder interferometer. The beam

passes through an interference filter and then it is focused by a lens, impinges on the Kwiat source and the process of SPDC occurs, generating the first pair of photons. To generate the second pair, the fundamental laser beam is reflected on a mirror **MM** and enters the BBO crystals from the other side. Photons generated from the process of SPDC are directed using prisms and mirrors and collected into single-mode optical fibers by fiber couplers. To restrict the range of wavelengths and avoid the residue of the pumping beam, the fiber couplers are equipped with interference filters. Fiber couplers are mounted on the stage. The movement of the stage is provided by screws, enabling manual translation in x, y and z directions (with micrometer accuracy) as well as the horizontal and vertical tilt. Thus, the maximum signal is collected into the fibers and they lead to the single-photon APDs, which are connected with coincidence counter. Within experimental setup, there are several iris diaphragms with adjustable opening deployed (with circular shape of aperture) that, except attenuation, are also used for beam alignment. In case of HOM interference measurement, two outputs of the fiber couplers (depending on the test case) are guided into a fiber beam splitter through the manual polarization controllers.

3.2 Adjustment

In the initial stages of aligning the experiment, precise adjustments of the laser system and second-harmonic generation unit were imperative. Assuring that the laser system and SHG unit generate the desired wavelength was the first step, requiring monitoring with a spectrometer. The fine-tuning of the crystal in the SHG unit while simultaneously controlling the output power and monitoring the wavelength peak was crucial for achieving the desired results. However, an unexpected outcome surfaced during these adjustments. It was discovered that, despite the SHG unit's declaration of filtering out the pump beam, a residue of the funda-

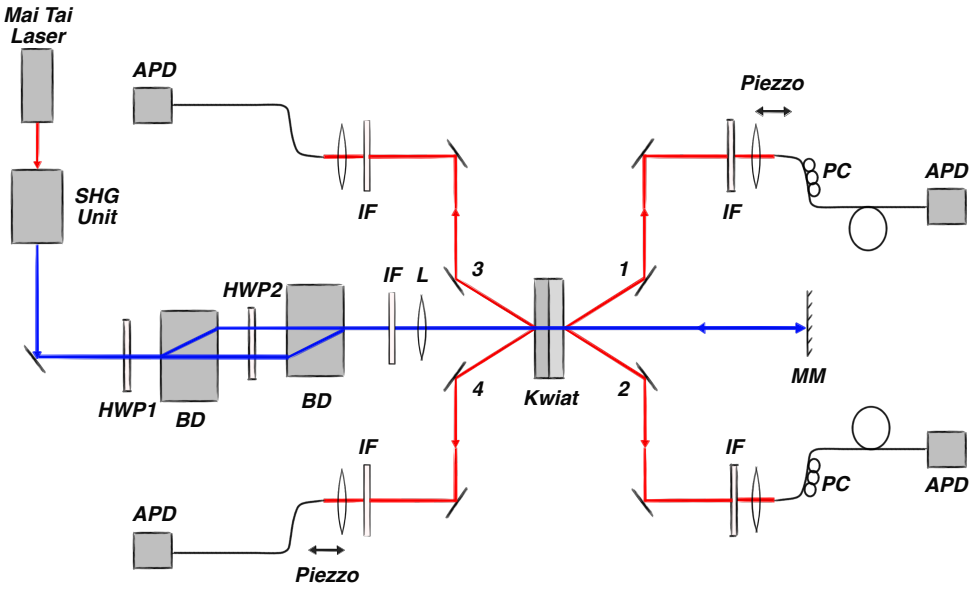

Figure 3.1: The scheme of the setup, where the components are labeled as: L - lens, APD - photon counter module, HWP - half-wave plate, IF - interference filter, BD - beam displacer, MM - mirror and PC - polarization controller.

mental infrared radiation beam persisted at the output of the SHG unit. It acted as an additional noise which thus obscured the generated photon pairs. This was not the only problem that we faced during adjusting of the SHG unit. It was discovered that the crystal inside the unit was burned through, so it was not possible to reach 2nd-harmonic frequency. It was necessary to order a new crystal and tune the angle again, which led to further delays.

To align the pumping beam path of propagation, all lenses are removed and the beam is propagated through the center of the irises all its way to the mirror by controlling the tilt of mirrors at the output of the SHG and in front of BD. It is important to align the propagation up to the mirror MM that reflects the fundamental beam back to the Kwiat from the opposite side. Note that tracing the beam in the backwards propagation using the position adjustment and the tilt of the mirror MM is essential as well.

For the rough positioning of tilt and positions of the fiber couplers, the laser is turned off and a signal from the semiconductor laser is connected to the fiber couplers from the other side (note that IF filters must be taken off the couplers during this step). By tuning the positions of couplers and mirrors, one is able to direct the beam to reflect on the prisms and to propagate through the center of the Kwiat source in the reverse direction.

In the context of searching for a signal for the first time, using edge filters placed on the fiber couplers can help to isolate and identify the desired signal.

In order to generate entangled photons, the wave plates that we mentioned in the section 3.1 must be set to modify the polarization of pumping beam. Nevertheless, in our setup, we are not focused on generation of polarization entangled photon pairs, so we postponed this part of adjustment and only set the polarization by rotation of a HWP_1 to horizontal/vertical polarization.

While the generation of polarization entangled photon pairs is not within our current intention, establishment of input polarization of the pumping beam remains crucial for the efficient generation of photon pairs and the observation of high-visibility interference patterns. To achieve this, polarization controllers are attached to the fibers guiding the beam towards the fiber beam splitter (note that the polarization controllers are used only in the case of HOM interference measurement). This enables us to ensure that the interacting photons closely approximate Fock states and are indistinguishable in both polarization and frequency.

3.3 Test Cases

When the placement of all the components and adjustment of the beam direction is complete, several test cases are performed. The test cases are based on the HOM interference (as described in section 2.7), where the photons in different modes are led to interfere on the fiber beam

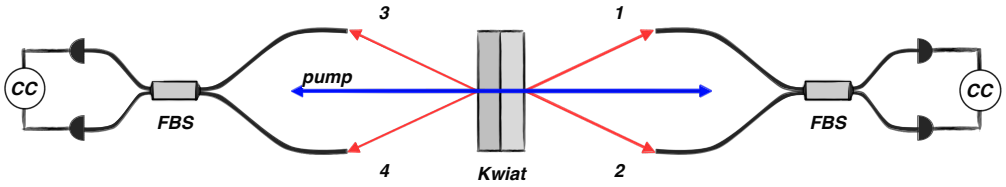

Figure 3.2: The scheme of the HOM interference measurement between the photons of identical pairs.

splitter and coincidence events are detected. As a default, interference filters of the 5 nm width are attached to the fiber couplers for all the test cases. In the case of interference between photons of identical pair, the various spectral widths of interference filters were used (see paragraph 3). In order to detect the coincidence events, the photons generated by the source must fulfill, except polarization and frequency, indistinguishability in time arrival to the fiber beam splitter.

3.3.1 Two-photon interference between photons of identical pair

The time indistinguishability of generated photon pairs is secured by using comparable length of the optical fibers, that lead to the beam splitter, and movement by one of the fiber couplers, so that the two photons of generated pair travel the same distance to the FBS. To make sure that the generated photon pairs are not distinguishable, we performed the HOM interference (as written in section 2.7) for both, the forward and backward photon pairs, respectively, as depicted in Figure 3.2.

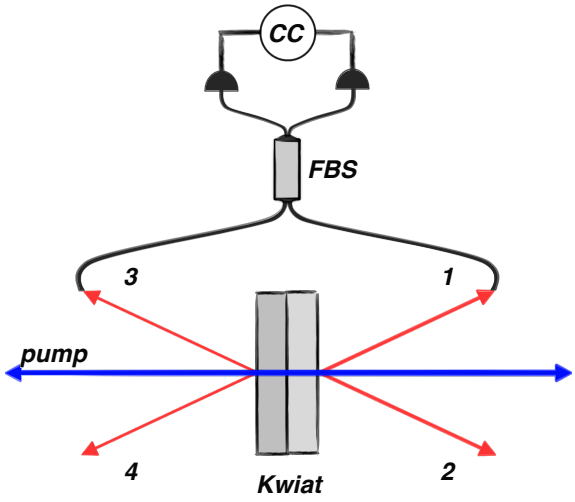

Figure 3.3: The scheme of the HOM two-photon interference measurement between the photons of different pairs.

3.3.2 Two-photon interference between photons of different pairs

In the previous test case, we focused on the interference between the photons originating in the same photon pair. Nevertheless, for many quantum information processing protocols, there is often requirement of more-photon interaction, so the interference between the photons of different pairs is interesting to test. In this case, we overlap one photon from the forward generated photon pair and one from the backward photon pair. We added a fiber beam splitter leading to the detectors to the propagation path and let the two photons from different photon pairs in modes 1 and 3 interfere according to the scheme in Figure 3.3. The HOM interference visibility is limited by multiphoton contributions, originating from the probability of coupling either two forward-generated photons and none of the backward-generated photons or vice versa.

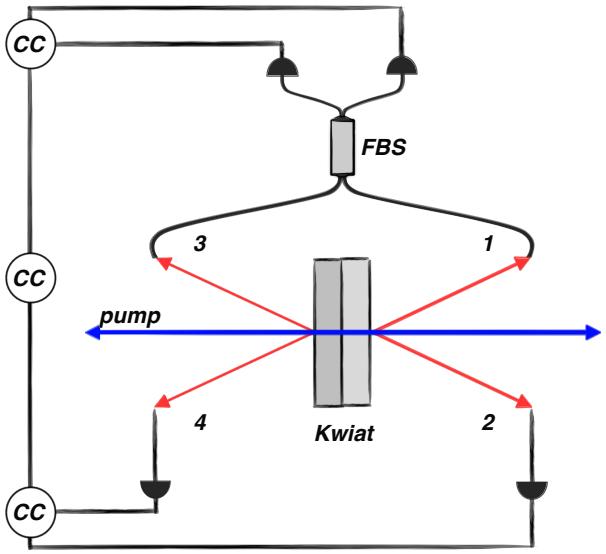

Figure 3.4: The scheme of the heralded HOM two-photon interference between photons of different pairs.

3.3.3 Heralded two-photon interference between photons of different pairs

The probability of multiphoton contributions can be reduced by suitable heralding. In this case, we overlapped the two photons in modes 1 and 3 as in the previous test case, but moreover, we led simultaneously the photons from the modes 2 and 4 to the detectors as depicted in the scheme (see Figure 3.4). Therefore, detecting a photon in mode 2 indicates the existence of a photon in mode 1 and apparently detecting a photon in mode 4 indicates the existence of a photon in mode 3.

Chapter 4

Results

In this chapter, the presented model of four-photon source is subjected to a set of test cases described in previous section 3.3. Firstly, the setup adjustments need to be performed as described in the section 3.2. Then, the HOM interference can be investigated. The coincidence window was set to 5 ns. Setting a longer coincidence window would increase the multiphoton contributions. The laser power entering the BBO crystal was approximately 215 mW. The visibilities of all HOM dips were calculated using the equation (2.26) and the measured data were fitted using the Gaussian function. The results of the HOM interference measurement in dependence on the test case are summarized below.

4.1 Two-photon interference between photons of identical pair

We tested the two-photon interference between photons of identical pair according to the description in section 3.3.1. We have measured HOM dips between photons 1 and 2 and between photons in modes 3 and 4 by adding a fiber beam splitter into the propagation path of the generated photon pairs. We let them interfere on the beam splitter and then detected coincidence counts while simultaneously moving with one of the

fiber couplers. The visibilities we have observed were 90% and 89%, respectively. The dip measurements are graphically depicted in Figures 4.1 and 4.2.

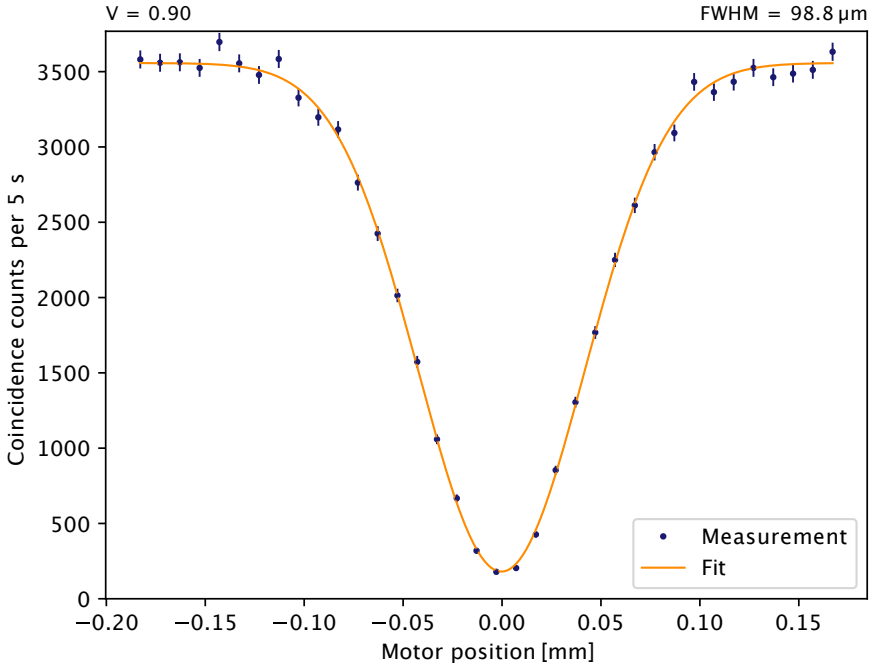

Figure 4.1: The HOM dip measured between the photons of the photon pairs that are generated in the forward direction (modes 1 and 2).

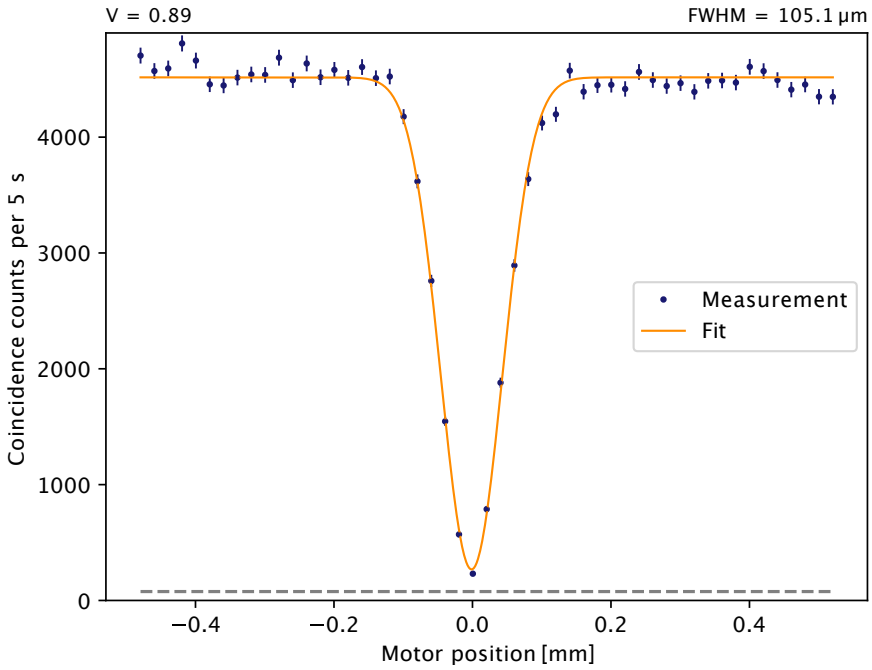

Figure 4.2: The HOM dip measured between the photons of the photon pairs that are generated in the backward direction (modes 3 and 4). The horizontal dashed line shows the level of multiphoton contributions.

As mentioned in the section 3.3, for the case of backward generated photon pairs, the HOM dip measurement was performed with various widths of interference filters. With an increase in the spectral width of interference filters, we observed a decrease in the FWHM value of the measured dips, as expected. The Figure 4.3 presents a depiction of the dip measurement for all HOM dips. For a summary of calculated values of FWHM and visibilities see Table 4.1. For this test case, we subtracted coincidence counts corresponding to the multiphoton contributions and included the resulting visibility values in the table (labeled as V_i).

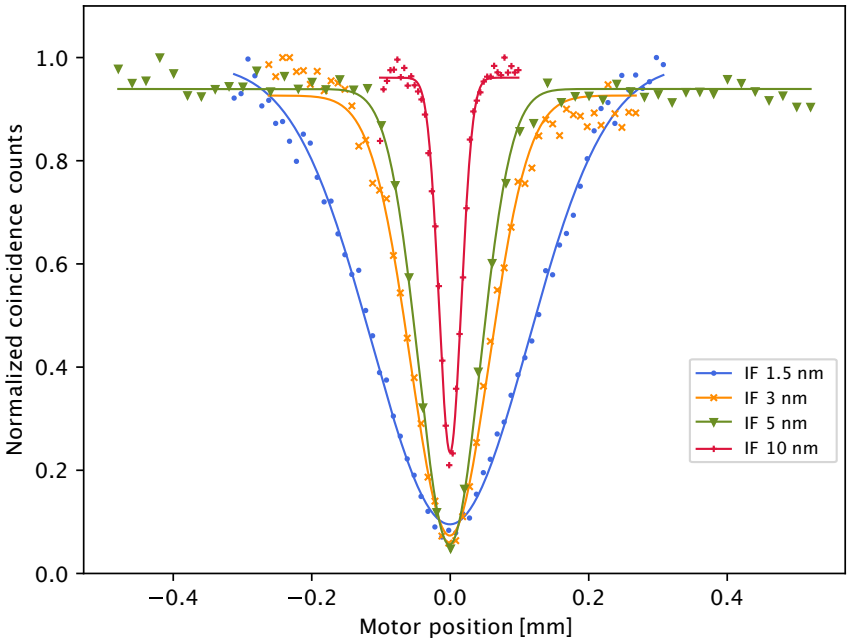

Figure 4.3: The measurement of HOM dip of the backward-generated photon pairs using interference filters of various spectral widths.

Table 4.1: The summary of HOM dip properties for the backward-generated photon pairs with various spectral widths of interference filters.

IF [nm]	FWHM [µm]	V [%]	V_i [%]
1.5	261.2	82	97.5
3	133.1	85	92.0
5	105.1	89	96.5
10	37.8	61	78.0

4.2 Two-photon interference between photons of different pairs

The indistinguishability between generated photons of different pairs was tested according to the description in section 3.3.2. HOM dips were measured between photons 1 and 3 and the results are summarized in Figure 4.4. Nevertheless, the HOM dip visibility is only 4%.

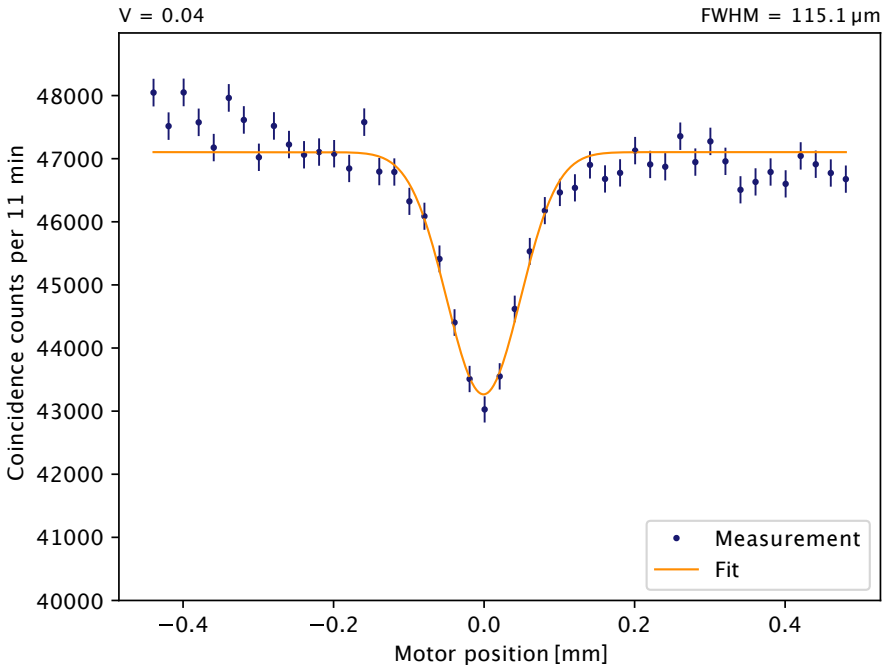

Figure 4.4: The HOM dip of cross-pair interference measurement. Note that the y-axis range does not start from zero.

4.3 Heralded two-photon interference between photons of different pairs

According to the description in section 3.3.3, we investigated HOM interference between photons 1 and 3 as in the previous test case, but this time with the photons from modes 2 and 4 detection. This improves the HOM dip visibility to 18%. In Figure 4.5 the test case results are presented.

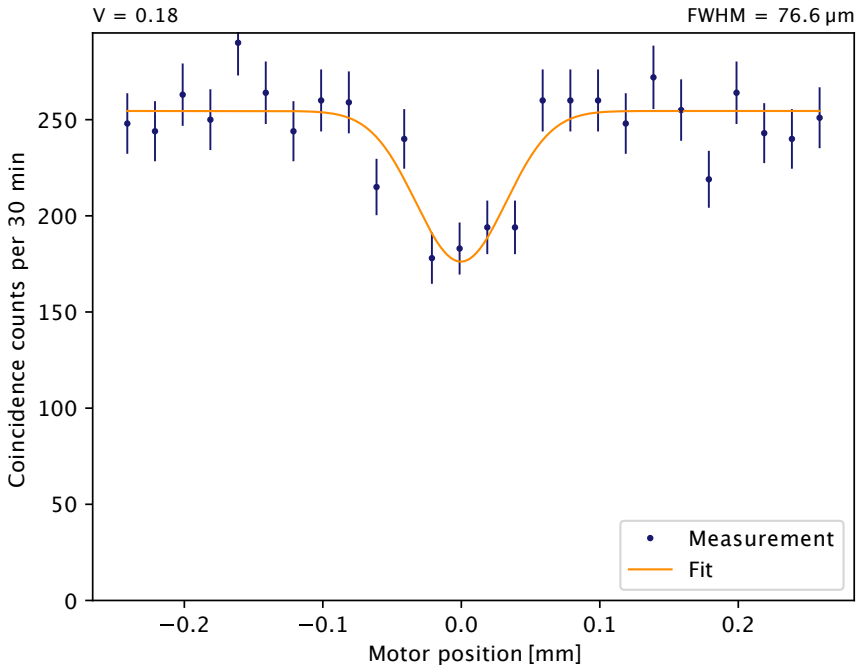

Figure 4.5: Observed Hong-Ou-Mandel cross-pair interference in modes 1 and 3, heralded by the simultaneous detection of photons in modes 2 and 4.

As the final step, we performed heralded HOM interference using the same method as before. However, this time we collected 16 measurements for a shorter time (10 minutes each), which we later merged and depicted in Figure 4.6. The visibility we achieved was 21% and approximately same FWHM value as in the previous case. We explain the low values of visibilities by the over-high pumping power. Unfortunately, the neutral-density filters, which are normally used to attenuate light, were burned through during the initial adjustment so we decided not to use them.

Besides the pumping power regulation, another possible enhancement lies in better polarization controlling of both modes interacting, so that the overlap on the beam splitter is perfect. Note that also a choice of a beam splitter itself with proper splitting ratio plays a crucial role in the HOM interference measurement.

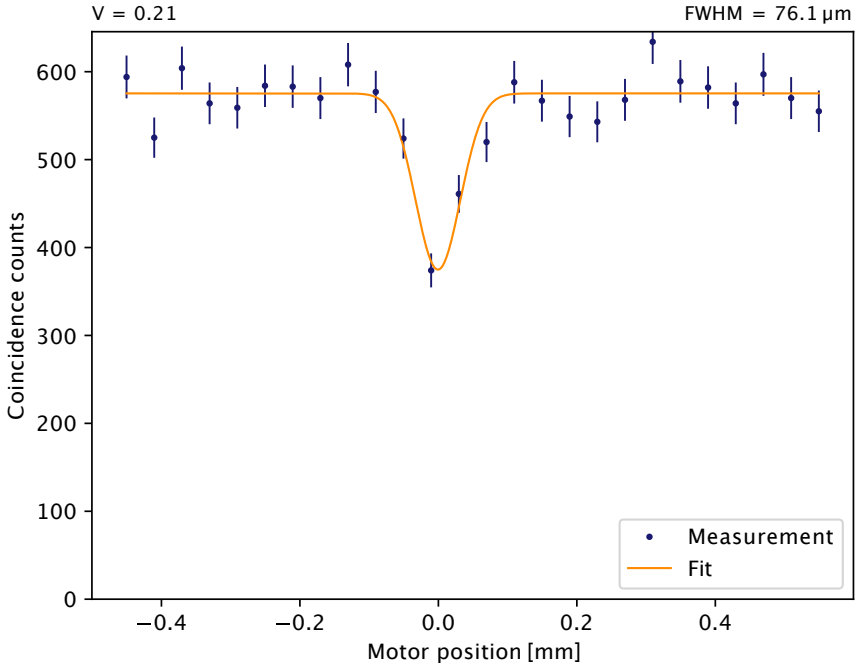

Figure 4.6: Merged HOM dip observed by interference in modes 1 and 3, heralded by the simultaneous detection of photons in modes 2 and 4.

Chapter 5

Conclusions

In this thesis, we have theoretically described and experimentally demonstrated the working principle of the 4PS based on the process of spontaneous parametric down-conversion with the Hong-Ou-Mandel interference testing. We have also outlined its potential applications, including further possible steps to improve the source setup.

More specifically, in the first part of this thesis, we have provided an introduction to our motivation behind undertaking this work. We have given a brief historical overview of the quantum physics, laser physics and introduced relevant basic principles.

Furthermore, in Chapter 2 we have presented a detailed description of the methods and tools used in this research. This includes a description of the basics of nonlinear optics. Additionally, we have explained various nonlinear optical processes such as spontaneous parametric down-conversion, second-harmonic generation, and Hong-Ou-Mandel interference, which are crucial in understanding the research work. Overview of the experimental setup, including all the crucial steps of the four-photon source construction is provided in Chapter 3. In this chapter, we start with the description of concrete optical components and general presentation of the four-photon source setup as well as the alignment of the whole setup and all the test cases are introduced.

In the final chapter, we present the results of our test cases, which demonstrate the indistinguishability of both forward and backward generated photon pairs by performing HOM interference on a beam splitter. The results of our experiments show that the coincidence counts tend to drop to zero. Both forward and backward-generated photon pairs had a measured visibility of around 90%, indicating the indistinguishability between the photons of identical pairs. Moreover, after the subtraction of counts corresponding to the multiphoton contributions, the visibility of the dip for the backward-generated photon pairs increased up to 96.5% as compared to the value obtained for the 5 nm interference filter. In the case of HOM interference between the photons of different pairs, the achieved visibility was only 4%. By proper heralding of the cross-pair interference, we achieved the HOM dip visibility of 21%. We consider our results to be satisfactory in demonstrating the proof of concept of our setup providing an opportunity for further possible improvements.

Bibliography

[1] M. Planck. *The Theory of Heat Radiation*. Dover Books on Physics Series. Dover Publications, 1991. ISBN: 9780486668116. URL: https://books.google.cz/books?id=UnGPVwLybcEC.

[2] Albert B. Einstein. "Concerning an heuristic point of view toward the emission and transformation of light". In: URL: https://api.semanticscholar.org/CorpusID:37804189.

[3] P. Zoller, Th. Beth, and D. Binosi. "Quantum information processing and communication". In: *The European Physical Journal D - Atomic, Molecular, Optical and Plasma Physics* 36.2 (2005). DOI: 10.1140/epjd/e2005-00251-1. URL: https://doi.org/10.1140/epjd/e2005-00251-1.

[4] Michael A. Nielsen and Isaac L. Chuang. *Quantum Computation and Quantum Information: 10th Anniversary Edition*. Cambridge University Press, 2010.

[5] Dik Bouwmeester et al. "Experimental quantum teleportation". In: *Nature* 390.6660 (1997), pp. 575–579. ISSN: 1476-4687. DOI: 10.1038/37539. URL: http://dx.doi.org/10.1038/37539.

[6] Maximilian Schlosshauer. "Quantum decoherence". In: *Physics Reports* 831 (2019). Quantum decoherence, pp. 1–57. ISSN: 0370-1573. DOI: https://doi.org/10.1016/j.physrep.2019.10.001. URL: https://www.sciencedirect.com/science/article/pii/S0370157319303084.

[7] R. J. Collins et al. "Quantum key distribution system in standard telecommunications fiber using a short wavelength single photon source". In: *Journal of Applied Physics* 107.7 (2010). ISSN: 1089-7550. DOI: 10.1063/1.3327427. URL: http://dx.doi.org/10.1063/1.3327427.

[8] Koji Azuma et al. “Quantum repeaters: From quantum networks to the quantum internet”. In: *Reviews of Modern Physics* 95.4 (2023). ISSN: 1539-0756. DOI: 10.1103/revmodphys.95.045006. URL: http://dx.doi.org/10.1103/RevModPhys.95.045006.

[9] Klaus Mattle et al. “Dense Coding in Experimental Quantum Communication”. In: *Phys. Rev. Lett.* 76 (25 1996), pp. 4656–4659. DOI: 10.1103/PhysRevLett.76.4656. URL: https://link.aps.org/doi/10.1103/PhysRevLett.76.4656.

[10] Ryszard Horodecki et al. “Quantum entanglement”. In: *Rev. Mod. Phys.* 81 (2 2009), pp. 865–942. DOI: 10.1103/RevModPhys.81.865. URL: https://link.aps.org/doi/10.1103/RevModPhys.81.865.

[11] Dmitry Makarov. “Theory for the Beam Splitter in Quantum Optics: Quantum Entanglement of Photons and Their Statistics, HOM Effect”. In: *Mathematics* 10.24 (2022). ISSN: 2227-7390. DOI: 10.3390/math10244794. URL: https://www.mdpi.com/2227-7390/10/24/4794.

[12] Bahaa E. A. Saleh and Malvin Carl Teich. *Fundamentals of photonics*. John Wiley & Sons, 2019.

[13] Charles H. Bennett and Gilles Brassard. “Quantum cryptography: Public key distribution and coin tossing”. In: *Theoretical Computer Science* 560 (2014). Theoretical Aspects of Quantum Cryptography – celebrating 30 years of BB84, pp. 7–11. ISSN: 0304-3975. DOI: https://doi.org/10.1016/j.tcs.2014.05.025. URL: https://www.sciencedirect.com/science/article/pii/S0304397514004241.

[14] Charles H. Bennett et al. “Teleporting an unknown quantum state via dual classical and Einstein-Podolsky-Rosen channels”. In: *Phys. Rev. Lett.* 70 (13 1993), pp. 1895–1899. DOI: 10.1103/PhysRevLett.70.1895. URL: https://link.aps.org/doi/10.1103/PhysRevLett.70.1895.

[15] Logan E. Hargrove, Richard Fork, and Martin Alan Pollack. “Locking of He–Ne laser modes induced by by synchronous intracavity modulation”. In: *Applied Physics Letters* 5 (1964), pp. 4–5. URL: https://api.semanticscholar.org/CorpusID:119023598.

[16] Robert W. Boyd. *Nonlinear Optics, Third Edition*. 3rd. USA: Academic Press, Inc., 2008. ISBN: 0123694701.

[17] J. Noda, K. Okamoto, and Y. Sasaki. "Polarization-maintaining fibers and their applications". In: *Journal of Lightwave Technology* 4.8 (1986), pp. 1071–1089. DOI: 10.1109/JLT.1986.1074847.

[18] Antonín Černoch et al. "Experimental implementation of partial symmetrization and anti-symmetrization of two-qubit states". In: *New Journal of Physics* 11.2 (2009), p. 023005. DOI: 10.1088/1367-2630/11/2/023005. URL: https://dx.doi.org/10.1088/1367-2630/11/2/023005.

[19] Paul G. Kwiat et al. "Ultrabright source of polarization-entangled photons". In: *Phys. Rev. A* 60 (2 1999), R773–R776. DOI: 10.1103/PhysRevA.60.R773. URL: https://link.aps.org/doi/10.1103/PhysRevA.60.R773.

[20] Excelitas Technologies. *SPCM-AQRH-14-FC*. PHOTON COUNT MODULE 100CPS FC. 2020. URL: https://www.digikey.be/en/products/detail/excelitas-technologies/SPCM-AQRH-14-FC/5885849.

[21] B. Ndagano and A. Forbes. "Entanglement distillation by Hong-Ou-Mandel interference with orbital angular momentum states". In: *APL Photonics* 4.1 (2019), p. 016103. ISSN: 2378-0967. DOI: 10.1063/1.5079970. eprint: https://pubs.aip.org/aip/app/article-pdf/doi/10.1063/1.5079970/13268230/016103_1_online.pdf. URL: https://doi.org/10.1063/1.5079970.

[22] Karol Bartkiewicz, Antonín Černoch, and Karel Lemr. *Experimental construction of a versatile four-photon source*. 2018. arXiv: 1808.07073 [quant-ph].

[23] Spectra-Physics. *Ultrafast One Box Ti:Sapphire Lasers*. Mai Tai. 2023. URL: https://www.spectra-physics.com/mam/celum/celum_assets/resources/Mai-Tai-Datasheet.pdf?3.

[24] Thorlabs. *PM100D - Compact Power and Energy Meter Console, Digital 4" LCD*. https://www.thorlabs.com/thorproduct.cfm?partnumber=PM100D. 2023.

[25] Thorlabs. *S302C - Thermal Power Sensor head, Surface Absorber, 100 μW – 2 W*. https://www.thorlabs.com/thorProduct.cfm?partnumber=S302C. 2018.

[26] Tausand electronic. *Tausand Abacus AB1000 coincidence counter*. https://www.tausand.com/downloads/user-manuals/. 2024.

List of Figures